AIAA JOURNAL
Vol. 36, No. 10, October 1998

Edge Effects in Laminated Composites with Pin-Loaded Holes

Chao Zhang,* Suong V. Hoa,† and R. Ganesan‡
Concordia University, Montreal, Quebec H3G 1M8, Canada

An analytical technique is developed for determining the three-dimensional edge effect stresses around pin-loaded holes in symmetric laminated composites. Based on the superposition principle of linear elasticity theory, the stress state around pin-loaded holes is divided into two parts, one the in-plane stress state determined using the classical laminated plate theory and the other the boundary-layer stress state arising from the edge effects that only exist in the vicinity of the holes. The equilibrium equations for boundary-layer stress state with zeroth-order approximation are written based on a set of power series expansions. A closed-form solution for the boundary-layer stress state with zeroth-order approximation is then obtained by imposing stress functions on the variational principle of complementary energy. Numerical results obtained using the present technique for cross-ply laminates are in good agreement with those obtained using finite element methods.

Nomenclature

$A^{(i)}, B^{(i)}, C^{(i)}$	= parameters related to the stress functions
$F^{(i)}(\xi, \eta)$, $G^{(i)}(\xi, \eta)$	= stress functions for the ith ply
f_i, g_i, h_i	= parameters used in the complementary energy principle
$f_{(i)}(\xi, \eta, \theta)$	= boundary-layer stress coefficients
H	= laminate thickness
h	= ply thickness
n	= number of plies in a laminate
$p^{(i)}(\eta), q^{(i)}(\eta)$	= functions for boundary-layer stress distribution along the ply thickness direction in the ith ply
R	= radius of pin-loaded holes
$S_{ij}^{(i)}$	= material compliances in the cylindrical coordinate system
u_{r0}^{c}	= radial displacement at the contact surfaces
α, β, γ	= real and positive parameters
Γ	= functional
ε^{c}	= laminate strains obtained from the classical laminated plate theory (CLPT)
ε_0^{c}	= laminate strains along hole edges obtained from the CLPT
$\varepsilon^{e(i)}$	= boundary-layer strains in the ith ply
$\varepsilon^{(i)}$	= total strains in the ith ply
λ	= root of characteristic equations
ξ, η	= dimensionless variables in the radial and thickness directions, respectively
Π	= complementary energy
$\sigma^{c(i)}, \tau^{c(i)}$	= in-plane stresses obtained from the CLPT in the ith ply
$\sigma^{e(i)}, \tau^{e(i)}$	= boundary-layer stresses in the ith ply
$\sigma^{(i)}, \tau^{(i)}$	= total stresses in the ith ply
σ_{r0}^{c}	= average in-plane radial stress across the laminate thickness along hole edges
$\sigma_0^{c(i)}, \tau_0^{c(i)}$	= in-plane stresses along hole edges obtained from the CLPT in the ith ply
$\Phi(\xi), \Psi(\xi)$	= common functions for boundary-layer stress distribution along the radial direction
$\Phi^{(i)}(\xi), \Psi^{(i)}(\xi)$	= functions for boundary-layer stress distribution along the radial direction in the ith ply

Received Sept. 19, 1997; revision received June 16, 1998; accepted for publication June 29, 1998.

*Ph.D. Candidate, Concordia Centre for Composites, Department of Mechanical Engineering.
†Professor and Director, Concordia Centre for Composites, Department of Mechanical Engineering.
‡Assistant Professor, Concordia Centre for Composites, Department of Mechanical Engineering.

Introduction

THREE-DIMENSIONAL edge effects predominantly responsible for the failure of laminated composite pinned joints used in transferring in-plane loads have been recognized for the past 20 years, since Quinn and Matthews[1] experimentally showed the influence of stacking sequence on the pin-bearing strength in glass fiber-reinforced plastics. This phenomenon is attributed to the existence of concentrated interlaminar stresses around pin-loaded holes in laminated composites. In spite of this recognition, most previous research in this field was performed on the basis of two-dimensional assumptions to avoid the complexity of three-dimensional stress analysis.[2–4] A three-dimensional stress and failure analysis can be expected to provide more information about the composite pinned/bolted joints because out-of-plane effects are considered in the modeling.[1,5,6] To date, only Shokrieh and Lessard[7] have undertaken a complete three-dimensional stress analysis in conjunction with a progressive damage model for the failure analysis of composite pinned joints. Further research is, therefore, required, especially on the aspects of three-dimensional stress analysis around pin-loaded holes in laminated composites.

Curved edge effects in laminated composites with traction-free circular holes have been studied in a few research works through numerical and analytical solution techniques. The finite element approach has been one of the most commonly used numerical techniques in past investigations. Rybicki and Schmueser[8] investigated the effect of stacking sequence and lay-up angle on the free edge stresses around circular holes, whereas Lucking et al.[9] investigated the effect of the hole radius to laminate thickness ratio on the interlaminar stresses in a $[0/90]_s$ composite. Both studies made use of the conventional three-dimensional displacement formulated isoparametric elements based on the potential energy principle. Ericson et al.[10] used singular elements with assumed strain field to treat the interlaminar stress concentration along hole free edges. Some special finite element techniques have also been developed to perform the stress analysis for the curved free edge problem. Nishioka and Atluri[11] proposed an assumed-stress hybrid finite element method based on the modified complementary energy principle, wherein the approach is to embed analytical asymptotic solutions into the special-hole elements. More recently, Hoa and Feng[12] developed a global/local approach using partial hybrid elements, in which the domain of laminated composites with curved free edges is divided into a local region, a transition region, and a global region to reduce the number of active degrees of freedom without loss of accuracy. The finite element methods, however, have suffered from the difficulties of handling the curved free edge effects in thick laminated composites due to the limitation of computing costs. Furthermore, caution must be taken when conventional displacement formulated isoparametric elements are used to model free edge problems, because it is believed that unreliable results of calculated stresses may arise from the inability to exactly satisfy the traction-free

conditions at free edges and traction-continuity conditions at layer interfaces.[13,14]

On the other hand, analytical closed-form solutions are preferable to define the potentially high interlaminar stress gradient field near circular-hole free edges of laminated composites. Unfortunately, the curved edge effects constitute a fully three-dimensional problem, so that it is very difficult if not impossible to find stress or displacement functions that satisfy the three-dimensional equilibrium and compatibility equations in a cylindrical coordinate system. Therefore, the boundary-layer theory, originally proposed by Reiss[15] for isotropic plates with circular holes and then extended to laminated composites by Tang,[16,17] is frequently employed as a powerful tool in the analysis of curved free edge effect.[18–20] In the boundary-layer theory, a small variable is introduced so as to yield the simplified equilibrium and compatibility equations with zeroth-order approximation, thereby making it possible to find stress functions (or displacement functions) for these simplified equations. Tang[16,17] developed zeroth-order solutions for curved free edge effects in thin laminated composites with only parts of the boundary conditions being guaranteed in an average sense. Ko and Lin[19] and Zhang et al.[20] obtained the zeroth-order solutions for curved free edge effects in both thin and thick laminated composites using the principle of complementary energy, in which all of the traction-free and traction continuity conditions at ply interfaces are exactly satisfied.

Compared with the edge effects of traction-free circular holes, relatively few research works have been conducted on the edge effect problems of pin-loaded holes in laminated composites because of the extreme complexity of boundary conditions at the pin–composite contact interface. Currently, no analytical closed-form solutions are available to predict the three-dimensional stresses in laminated composite pinned/bolted joints. A number of researchers have devoted their efforts to this problem using fully three-dimensional finite element techniques.[5,7,21–23] However, the fully three-dimensional finite element analysis requires a large amount of computer storage and run time, thereby making it rather difficult to obtain accurate results. As a matter of fact, most of their works are restricted to the cases of $[0/90]_s$ and $[90/0]_s$ cross-ply laminates. Matthews et al.[5] developed a 20-node isoparametric brick element consisting of a number of layers to compute the edge effects in multidirectional laminates. Sperling[21] and Marshall et al.[22] made use of high-order displacement formulated elements with coarse meshing for the problem of edge effects. Recently, Shokrieh and Lessard[7] and Lessard et al.[23] formed a computational model that includes more 20-node isoparametric brick elements through the thickness of each layer so as to achieve higher accuracy in the quantification of the edge effects in cross-ply laminates. By performing a mesh-dependence study, they[7,23] showed that element meshing is of great importance for the results of edge effects in finite element analysis. As a result, Sperling[21] and Marshall et al.[22] reported that the interlaminar shear stresses are smaller than the interlaminar normal stress around pin-loaded holes in cross-ply laminates, but Shokrieh and Lessard[7] and Lessard et al.[23] established a conclusion to the contrary. Therefore, reliable results for the curved edge effect problem can be obtained from finite element analysis only when the element meshing is fine enough.

The objective of the present paper is to develop elastic solutions for three-dimensional edge effect stresses around pin-loaded holes in symmetric laminated composites. The variational approach developed by Zhang et al.[20] for the problem of curved free edge effects is further extended and employed in the present work. The contact interactions between the pin and the hole are simulated by applying prescribed radial displacement boundary conditions on the contact surface and traction free conditions on the no-contact surface. Similar to most research on composite pinned joints,[5,7,21–23] the friction effects between pin and hole surfaces are neglected, thus making the contact surfaces free of shear traction. Following the boundary-layer theory,[16] curved edge effect stresses can be approximately represented by a zeroth-order boundary-layer stress state, for which two stress functions are then determined by imposing the procedure of the calculus of variations on to the complementary energy of the elastic system. All of the traction-free conditions along the pin-loaded hole edges and traction-continuity conditions at ply interfaces are satisfied, whereas the radial displacement boundary conditions on the contact surfaces are approximately satisfied via natural boundary conditions obtained in the operation of the calculus of variations. The present solutions for edge effect stresses around pin-loaded holes have the simple forms of exponential functions, thus providing a computational tool for thick laminated composites with the advantages of being simple and efficient. Numerical illustrations of the interlaminar stresses in cross-ply laminated composites are also presented.

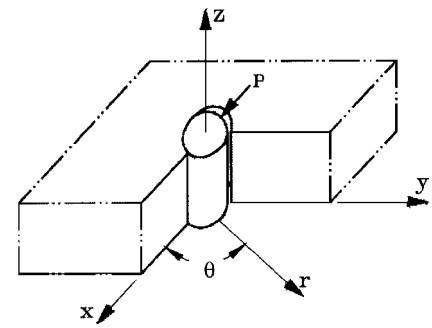

Fig. 1 Schematic representation of laminated composite pinned joints.

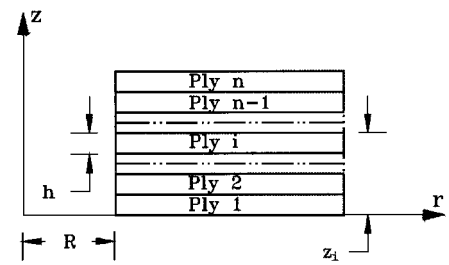

Fig. 2 Laminate geometry and construction.

Problem Description

The problem of interest consists of a symmetric laminate with a circular hole, to which a load P is applied by a pin, as shown in Fig. 1. The pin-loaded hole edge is divided into two regions. One is the contact surface where the pin and the hole edge are in contact, and the other is the no-contact surface where a clearance exists. The region of contact surface, i.e., contact angle, is determined by several factors, such as tolerance, material properties, loading, etc. The hole has a radius of R. The laminate is composed of n orthotropic and homogeneous plies with individual fiber orientations, and the thickness for each ply is h (Fig. 2); thus, the laminate thickness H is equal to nh. The origin of a cylindrical coordinate system is fixed at the center of the hole on the bottom surface of the laminate. Therefore, in the defined coordinate system, the interface between the ith and $(i+1)$th plies is located at $z_i = ih$, and it is defined that $z_0 = 0$.

To simplify the model formulation in the study, it is assumed that 1) the pin is infinitely rigid and 2) the laminate is infinitely large. The influence of these two common assumptions on the model simulation of composite pinned joints is unimportant. This is because the dimensions for edge and side distances of composite pinned joints are usually designed to be much larger than the radius of holes so that the joints fail in a bearing mode because this failure is not catastrophic.[24] Also, the effect of pin elasticity on the stress distribution around pin-loaded holes is usually neglected because the stiffness of metal pins is considerably larger than that of polymer–matrix composites.[25]

Solution Methodology

Previous research has shown that edge effects in laminated composites exist in the vicinity of edges (namely, the boundary-layer region).[16,17,19,20] Hence, it is not adequate to describe the mechanical behavior of the boundary-layer regions by the in-plane anisotropic elasticity theory[26] in conjunction with the classical laminated plate theory (CLPT). In fact, the in-plane anisotropic elasticity theory gives only average values of in-plane stresses over

laminate thickness, but out-of-plane stresses are ignored in the boundary-layer regions. Thus, based on the superposition principle of linear elasticity theory,[27] the stress and strain fields in the boundary-layer regions can be considered as the summation of two parts.[16,17,19,20,28,29] One is the in-plane state predicted by the CLPT, and the other is the additional three-dimensional state, hereafter referred to as the boundary-layer state, resulting from edge effects. For the problem of composite pinned joints, the average values of in-plane stresses and displacements over the laminate thickness can be calculated using Hyer and Klang's,[25] Zhang and Ueng's[30] or de Jong's[31] analytical solutions. Particularly, these in-plane anisotropic solutions give an accurate boundary condition for the radial displacement along the contact surface, where the radial displacement must be uniform across the laminate thickness, thus constituting a prescribed radial displacement boundary condition in the present model. Now the total stresses and strains in ply i are given by

$$\begin{aligned}
&\sigma_r^{(i)} = \sigma_r^{c(i)} + \sigma_r^{e(i)}, \qquad \varepsilon_r^{(i)} = \varepsilon_r^c + \varepsilon_r^{e(i)} \\
&\sigma_\theta^{(i)} = \sigma_\theta^{c(i)} + \sigma_\theta^{e(i)}, \qquad \varepsilon_\theta^{(i)} = \varepsilon_\theta^c + \varepsilon_\theta^{e(i)} \\
&\sigma_z^{(i)} = \sigma_z^{e(i)}, \qquad \varepsilon_z^{(i)} = \varepsilon_z^c + \varepsilon_z^{e(i)}, \qquad \tau_{zr}^{(i)} = \tau_{zr}^{e(i)} \\
&\varepsilon_{zr}^{(i)} = \varepsilon_{zr}^{e(i)}, \qquad \tau_{z\theta}^{(i)} = \tau_{z\theta}^{e(i)}, \qquad \varepsilon_{z\theta}^{(i)} = \varepsilon_{z\theta}^{e(i)} \\
&\tau_{r\theta}^{(i)} = \tau_{r\theta}^{c(i)} + \tau_{r\theta}^{e(i)}, \qquad \varepsilon_{r\theta}^{(i)} = \varepsilon_{r\theta}^c + \varepsilon_{r\theta}^{e(i)}
\end{aligned} \tag{1}$$

where the superscript c associated with σ and ε refers to the stresses and strains obtained from the CLPT. Therefore, the corresponding in-plane strains remain constant across the laminate thickness. In a similar manner, the superscript e refers to the boundary-layer stresses and strains arising from the edge effects, which satisfy the Hooke's constitutive relationships in the cylindrical coordinate system:

$$\begin{Bmatrix} \varepsilon_r^e \\ \varepsilon_\theta^e \\ \varepsilon_z^e \\ \varepsilon_{zr}^e \\ \varepsilon_{z\theta}^e \\ \varepsilon_{r\theta}^e \end{Bmatrix}^{(i)} = \begin{bmatrix} S_{11} & S_{12} & S_{13} & 0 & 0 & S_{16} \\ S_{12} & S_{22} & S_{23} & 0 & 0 & S_{26} \\ S_{13} & S_{23} & S_{33} & 0 & 0 & S_{36} \\ 0 & 0 & 0 & S_{44} & S_{45} & 0 \\ 0 & 0 & 0 & S_{45} & S_{55} & 0 \\ S_{16} & S_{26} & S_{36} & 0 & 0 & S_{66} \end{bmatrix}^{(i)} \begin{Bmatrix} \sigma_r^e \\ \sigma_\theta^e \\ \sigma_z^e \\ \tau_{zr}^e \\ \tau_{z\theta}^e \\ \tau_{r\theta}^e \end{Bmatrix}^{(i)} \tag{2}$$

In Fig. 1, there are several boundary conditions that need to be satisfied.

1) The top and bottom surfaces of the laminate are free of tractions, i.e., at $z = 0$

$$\sigma_z^{(1)} = 0, \qquad \tau_{z\theta}^{(1)} = 0, \qquad \tau_{zr}^{(1)} = 0 \tag{3a}$$

and at $z = H$

$$\sigma_z^{(n)} = 0, \qquad \tau_{z\theta}^{(n)} = 0, \qquad \tau_{zr}^{(n)} = 0 \tag{3b}$$

2) At any interface between two plies, traction continuity must be guaranteed. That is, at $z = z_i$ $(i = 1, \ldots, n-1)$

$$\sigma_z^{(i)} = \sigma_z^{(i+1)}, \qquad \tau_{zr}^{(i)} = \tau_{zr}^{(i+1)}, \qquad \tau_{z\theta}^{(i)} = \tau_{z\theta}^{(i+1)} \tag{3c}$$

3) The contact surface is only free of shear tractions but subjected to the boundary condition of a prescribed radial displacement u_{r0}^c determined by the in-plane anisotropic solutions,[25,30,31] whereas the no-contact region is free of tractions. That is, on contact surface $(r = R)$

$$\tau_{r\theta}^{(i)} = 0, \qquad \tau_{zr}^{(i)} = 0, \qquad u_r^{(i)} = u_{r0}^c \tag{3d}$$

and on no-contact surface $(r = R)$

$$\tau_{r\theta}^{(i)} = 0, \qquad \tau_{zr}^{(i)} = 0, \qquad \sigma_r^{(i)} = 0 \tag{3e}$$

4) Because edge effects only exist in the boundary-layer regions, the solution of the CLPT is recovered, and the boundary-layer stresses are, thus, equal to zero far from the hole edges, i.e., as $r \to \infty$

$$\sigma_\theta^{(i)} = \sigma_\theta^{c(i)}, \qquad \sigma_r^{(i)} = \sigma_r^{c(i)}, \qquad \tau_{r\theta}^{(i)} = \tau_{r\theta}^{c(i)} \tag{3f}$$

$$\sigma_z^{(i)} = 0, \qquad \tau_{z\theta}^{(i)} = 0, \qquad \tau_{zr}^{(i)} = 0 \tag{3g}$$

The displacement continuity conditions at ply interfaces are relaxed because the variational principle of complementary energy is employed in the present model.

The solution procedure employed to determine the boundary-layer stress state is described as follows:

1) Expand the boundary-layer stress state into a power series of a small dimensionless parameter.

2) Obtain the zeroth-order boundary-layer equilibrium equations based on this power series.

3) Assume the forms of boundary-layer stress functions that satisfy the zeroth-order equilibrium equations and parts of the boundary conditions.

4) As an approximation, the calculus of variations is performed only on the part of the complementary energy that is caused by the boundary-layer stress state,[19,20,28] and it is further assumed that the stress functions corresponding to the stationarity of the complementary energy can be regarded as the solutions to the boundary-layer stresses.

5) Determine the parameters in the boundary-layer stress functions by imposing the associated boundary conditions.

Variational Principle of Complementary Energy

The complementary energy of the present system can be written as

$$\Pi = \Pi_c + \frac{1}{2}\int_v \{\sigma^e\}^T [S] \{\sigma^e\}\, \mathrm{d}v + \int_v \{\sigma^e\}^T \{\varepsilon^c\}\, \mathrm{d}v - \int_s \{p^e\}^T \{\underline{u}\}\, \mathrm{d}s \tag{4}$$

where Π_c is the complementary energy resulting from the CLPT stress state, v is the domain in which the complementary energy is considered, and $\{p^e\}$ are the boundary-layer tractions applied to the boundary s with prescribed displacements $\{\underline{u}\}$. The first term is determined by the CLPT stress state, which is assumed to be independent of the boundary-layer stresses for mathematical convenience. The second term is the strain energy arising from the boundary-layer stress components. The third term is the work representing the coupling effect between the boundary-layer stresses and the CLPT strains, and the fourth term is the work done by boundary-layer tractions on the prescribed displacement boundary. In the analytical models of free edge effects, the contribution of the third term to the complementary energy is usually ignored to simplify the involved mathematical work.[19,20,28]

A. Boundary-Layer Equilibrium Equations

Because edge effects constitute a fully three-dimensional problem, each ply in the laminate is treated as a separate three-dimensional elastic body with all six stress components. The total stresses of the system are required to obey the three-dimensional equilibrium equations in the cylindrical coordinate system. Because the CLPT stress state, one part of the total stresses, has already satisfied the equilibrium conditions, this part can be removed from the equilibrium equations. Hence, only the boundary-layer stress state, another part of the total stresses, is kept in these equilibrium equations. This means that the equilibrium conditions can be guaranteed in the present system only if the boundary-layer stress state satisfies these equilibrium equations. Therefore, after introducing the following two dimensionless variables:

$$\xi = (r - R)/h, \qquad \eta = z/h \tag{5}$$

the equilibrium equations governing the ith ply only in terms of the corresponding boundary-layer stress state can be written as

$$\frac{1}{h}\frac{\partial \tau_{r\theta}^{e(i)}}{\partial \xi} + \frac{1}{\xi h + R}\frac{\partial \sigma_\theta^{e(i)}}{\partial \theta} + \frac{1}{h}\frac{\partial \tau_{z\theta}^{e(i)}}{\partial \eta} + \frac{2\tau_{r\theta}^{e(i)}}{\xi h + R} = 0 \tag{6a}$$

$$\frac{1}{h}\frac{\partial \sigma_r^{e(i)}}{\partial \xi} + \frac{1}{\xi h + R}\frac{\partial \tau_{r\theta}^{e(i)}}{\partial \theta} + \frac{1}{h}\frac{\partial \tau_{zr}^{e(i)}}{\partial \eta} + \frac{\sigma_r^{e(i)} - \sigma_\theta^{e(i)}}{\xi h + R} = 0 \quad (6b)$$

$$\frac{1}{h}\frac{\partial \tau_{zr}^{e(i)}}{\partial \xi} + \frac{1}{\xi h + R}\frac{\partial \tau_{z\theta}^{e(i)}}{\partial \theta} + \frac{1}{h}\frac{\partial \sigma_z^{e(i)}}{\partial \eta} + \frac{\tau_{zr}^{e(i)}}{\xi h + R} = 0 \quad (6c)$$

Following Refs. 15 and 16, the boundary-layer stresses may be expanded into a power series of a small parameter (h/R), such that $h/R \ll 1$,

$$\sigma^{e(i)} = \sum_{m=0}^{\infty} f_{(i)}^{(m)}(\xi, \eta, \theta)\left(\frac{h}{R}\right)^m \quad (7)$$

where the superscript m in $f_{(i)}^{(m)}(\xi, \eta, \theta)$ denotes the order and that in $(h/R)^m$ denotes the corresponding power. Substituting Eq. (7) into equilibrium equations (6) and comparing the terms with the equal power of h/R yield a series of equilibrium equations for boundary-layer stress coefficients[16]

$$\frac{\partial f_{r\theta(i)}^{(0)}}{\partial \xi} + \frac{\partial f_{z\theta(i)}^{(0)}}{\partial \eta} = 0 \quad (8a)$$

$$\frac{\partial f_{r(i)}^{(0)}}{\partial \xi} + \frac{\partial f_{zr(i)}^{(0)}}{\partial \eta} = 0 \quad (8b)$$

$$\frac{\partial f_{zr(i)}^{(0)}}{\partial \xi} + \frac{\partial f_{z(i)}^{(0)}}{\partial \eta} = 0 \quad (8c)$$

For $m \geq 1$, one sets

$$\frac{\partial f_{r\theta(i)}^{(m)}}{\partial \xi} + \frac{\partial f_{z\theta(i)}^{(m)}}{\partial \eta} + \xi\left(\frac{\partial f_{r\theta(i)}^{(m-1)}}{\partial \xi} + \frac{\partial f_{z\theta(i)}^{(m-1)}}{\partial \eta}\right) + \frac{\partial f_{\theta(i)}^{(m-1)}}{\partial \theta} + 2f_{r\theta(i)}^{(m-1)} = 0 \quad (9a)$$

$$\frac{\partial f_{r(i)}^{(m)}}{\partial \xi} + \frac{\partial f_{zr(i)}^{(m)}}{\partial \eta} + \xi\left(\frac{\partial f_{r(i)}^{(m-1)}}{\partial \xi} + \frac{\partial f_{zr(i)}^{(m-1)}}{\partial \eta}\right) + \frac{\partial f_{r\theta(i)}^{(m-1)}}{\partial \theta} + f_{r(i)}^{(m-1)} - f_{\theta(i)}^{(m-1)} = 0 \quad (9b)$$

$$\frac{\partial f_{zr(i)}^{(m)}}{\partial \xi} + \frac{\partial f_{z(i)}^{(m)}}{\partial \eta} + \xi\left(\frac{\partial f_{zr(i)}^{(m-1)}}{\partial \xi} + \frac{\partial f_{z(i)}^{(m-1)}}{\partial \eta}\right) + \frac{\partial f_{z\theta(i)}^{(m-1)}}{\partial \theta} + f_{zr(i)}^{(m-1)} = 0 \quad (9c)$$

The boundary-layer theory[16,19] has confirmed that the zeroth-order boundary-layer stress coefficients can approximately represent the boundary-layer stresses resulting from the edge effects in Eq. (1). The stress coefficient $f_{\theta(i)}^{(0)}$ drops out of equilibrium equations (8) but can be obtained by setting the boundary-layer circumferential strain $\varepsilon_\theta^{e(i)}$ to be zero[16,19] because curved edge effects do not cause additional circumferential strain, such as the case of traction-free circular holes numerically verified by Raju and Crews.[32] Therefore, from Hooke's constitutive relationships, one can obtain

$$f_{\theta(i)}^{(0)} = -\frac{S_{12}^{(i)} f_{r(i)}^{(0)} + S_{23}^{(i)} f_{z(i)}^{(0)} + S_{26}^{(i)} f_{r\theta(i)}^{(0)}}{S_{22}^{(i)}} \quad (10)$$

An important feature of the boundary-layer theory is that there are no partial derivative terms with respect to θ in the zeroth-order boundary-layer equilibrium equations. Hence, the mathematical operations to determine the six zeroth-order boundary-layer stress coefficients are not performed on the values of θ in the variational procedure of complementary energy. However, all of them still depend on θ and, thus, are functions of ξ, θ, and η. From this point onward, therefore, the θ dependence is not shown explicitly in the following equations for reasons of clarity. Moreover, the symbols for stress coefficients $f^{(0)}$ are hereinafter replaced by that for boundary-layer stresses σ^e.

B. Boundary-Layer Stress Functions

Equilibrium equations (8) can be identified as two groups. The first group consists of Eqs. (8b) and (8c). The stresses $\sigma_r^{e(i)}$, $\sigma_z^{e(i)}$ and $\tau_{zr}^{e(i)}$ in Eqs. (8b) and (8c) are considered to be the stress components in the z–r plane strain state. Therefore, these three stress components can be related by a function $F^{(i)}(\xi, \eta)$ that satisfies plane strain equilibrium equations. The second group consists of Eq. (8a). The stresses $\tau_{r\theta}^{e(i)}$ and $\tau_{z\theta}^{e(i)}$ are related by a stress function $G^{(i)}(\xi, \eta)$ that ensures the satisfaction of equilibrium equation (8a). Suppose that the stress functions on ξ and η can be separated according to

$$F^{(i)}(\xi, \eta) = \Phi^{(i)}(\xi)p^{(i)}(\eta) \quad (11)$$

$$G^{(i)}(\xi, \eta) = \Psi^{(i)}(\xi)q^{(i)}(\eta) \quad (12)$$

Then, the boundary-layer stress components can be written as

$$\sigma_r^{e(i)} = \frac{\partial^2 F^{(i)}}{\partial \eta^2} = \Phi^{(i)}(\xi)\frac{\mathrm{d}^2 p^{(i)}(\eta)}{\mathrm{d}\eta^2} \quad (13a)$$

$$\sigma_z^{e(i)} = \frac{\partial^2 F^{(i)}}{\partial \xi^2} = \frac{\mathrm{d}^2 \Phi^{(i)}(\xi)}{\mathrm{d}\xi^2}p^{(i)}(\eta) \quad (13b)$$

$$\tau_{zr}^{e(i)} = -\frac{\partial^2 F^{(i)}}{\partial \xi\, \partial \eta} = -\frac{\mathrm{d}\Phi^{(i)}(\xi)}{\mathrm{d}\xi}\frac{\mathrm{d}p^{(i)}(\eta)}{\mathrm{d}\eta} \quad (13c)$$

and

$$\tau_{r\theta}^{e(i)} = \frac{\partial G^{(i)}}{\partial \eta} = \Psi^{(i)}(\xi)\frac{\mathrm{d}q^{(i)}(\eta)}{\mathrm{d}\eta} \quad (14a)$$

$$\tau_{z\theta}^{e(i)} = -\frac{\partial G^{(i)}}{\partial \xi} = -\frac{\mathrm{d}\Psi^{(i)}(\xi)}{\mathrm{d}\xi}q^{(i)}(\eta) \quad (14b)$$

The stress component $\sigma_\theta^{e(i)}$ can be obtained from Eq. (10), i.e., $\sigma_\theta^{e(i)} = f_{\theta(i)}^{(0)}$.

For functions $p^{(i)}(\eta)$ and $q^{(i)}(\eta)$, the assumptions made in Refs. 19, 20, and 33–35 are adopted:

$$p^{(i)}(\eta) = \tfrac{1}{2}\eta^2 + A^{(i)}\eta + B^{(i)} \quad (15)$$

$$q^{(i)}(\eta) = \eta + C^{(i)} \quad (16)$$

where $A^{(i)}$, $B^{(i)}$, and $C^{(i)}$ are parameters that are determined for each ply. The preceding assumptions result in two in-plane boundary-layer stress components that are uniform through the ply thickness, that is, $\sigma_r^{e(i)} = \Phi^{(i)}(\xi)$ and $\tau_{r\theta}^{e(i)} = \Psi^{(i)}(\xi)$.

To satisfy the traction continuity conditions at every ply interface, functions $\Phi^{(i)}$ and $\Psi^{(i)}$ throughout the laminate thickness must be represented by a common function in each case and related parameters. Furthermore, because both the existence of boundary-layer stress state and the difference of CLPT stress state in each ply are attributed to the mismatch of relative elastic properties between individual plies, the two in-plane boundary-layer stress components are assumed to be proportional to their CLPT counterparts in each ply. Noting that $\sigma_{r0}^{c(i)}$ and $\tau_{r\theta 0}^{c(i)}$ (the subscript 0 represents the variables along the pin-loaded hole edge) are CLPT radial and shear stresses in the ith ply along the hole edge and that σ_{r0}^{c} is the average in-plane radial stress component across the laminate thickness along the hole edge, one can write

$$\sigma_r^{e(i)} = \Phi^{(i)}(\xi) = \left(\sigma_{r0}^{c(i)} - \sigma_{r0}^{c}\right)\Phi(\xi) \quad (17)$$

$$\tau_{r\theta}^{e(i)} = \Psi^{(i)}(\xi) = \tau_{r\theta 0}^{c(i)}\Psi(\xi) \quad (18)$$

wherein σ_{r0}^{c} is equal to zero on the no-contact surface. These assumptions, thus, yield a zero resultant for the two in-plane boundary-layer stresses over the laminate thickness. For the problem of free edge effects, similar assumptions have been made to constitute the stress functions.[19,20,28,35,36] Because of the assumptions in Eqs. (17) and (18), the restrictive conditions on contact surface in Eqs. (3) are changed as follows:

$$\Psi(0) = -1, \qquad \Phi'(0) = 0, \qquad u_r^{(i)}(0) = u_{r0}^{c} \quad (19a)$$

and on no-contact surface are changed as follows:

$$\Psi(0) = -1, \qquad \Phi'(0) = 0, \qquad \Phi(0) = -1 \tag{19b}$$

$$\Phi(\infty) = 0, \qquad \Phi'(\infty) = 0, \qquad \Phi''(\infty) = 0 \tag{19c}$$

$$\Psi(\infty) = 0, \qquad \Psi'(\infty) = 0 \tag{19d}$$

and the condition $\sigma_\theta^{(i)}(\xi \to \infty) = \sigma_\theta^{c(i)}$ is, thus, automatically satisfied, following the conditions in Eqs. (19c) and (19d).

From the assumptions regarding the stress functions, the parameters $A^{(i)}$, $B^{(i)}$, and $C^{(i)}$ in functions $p^{(i)}(\eta)$ and $q^{(i)}(\eta)$ are determined by enforcing the traction-continuity conditions at interfaces in Eq. (3c) and the traction-free conditions on the bottom and top surfaces of the laminate in Eqs. (3a) and (3b), as follows.[20] For the first ply

$$A^{(1)} = 0, \qquad B^{(1)} = 0, \qquad C^{(1)} = 0 \tag{20a}$$

and for the other plies, i.e., $i \geq 2$,

$$A^{(i)} = \frac{1}{\left(\sigma_{r0}^{c(i)} - \sigma_{r0}^{c}\right)} \sum_{k=1}^{i-1} \left(\sigma_{r0}^{c(k)} - \sigma_{r0}^{c}\right) - (i-1) \tag{20b}$$

$$B^{(i)} = -\frac{1}{\left(\sigma_{r0}^{c(i)} - \sigma_{r0}^{c}\right)} \sum_{k=1}^{i-1} \left[\frac{1}{2}\left(\sigma_{r0}^{c(k)} - \sigma_{r0}^{c}\right)(2k-1)\right] + \frac{(i-1)^2}{2} \tag{20c}$$

$$C^{(i)} = \frac{1}{\left(\tau_{r\theta 0}^{c(i)}\right)} \sum_{k=1}^{i-1} \left(\tau_{r\theta 0}^{c(k)}\right) - (i-1) \tag{20d}$$

Especially, it can be derived from the preceding equations that

$$A^{(n)} = -n, \qquad B^{(n)} = -n^2/2, \qquad C^{(n)} = -n \tag{20e}$$

Hence, although $p^{(i)}(\eta)$ and $q^{(i)}(\eta)$ in terms of higher-order-degree polynomials are preferable because a better accuracy can be expected for stress distribution across the laminate thickness, they are assumed to be a second- and a first-degree polynomials, respectively, in the present model so that all of the parameters related to them can be determined from the traction-continuity conditions at ply interfaces and the traction-free conditions on the surfaces of the laminate. Previous research[18–20,28,33–37] has verified that the lower-degree approximations in the laminate thickness direction can yield reliable values, especially for interlaminar shear stress component $\tau_{z\theta}$ at interfaces in the problem of curved free edge effects.

C. Governing Equations

As stated earlier, the mathematical operations are not performed on the values of θ in the variational procedure; therefore, the complementary energy can be considered in a domain of $0 \leq z \leq H$ and $R \leq r \leq \infty$ for all values of θ. Because the summation of the boundary-layer stress $\sigma_{r0}^{e(i)}$ is equal to zero over the laminate thickness, the fourth term in Eq. (4) is null in the present system, though the radial displacement, remaining uniform across the laminate thickness, is prescribed on the contact surface. After expanding the matrices, the complementary energy Π_e that results from the boundary-layer stress state, i.e., $\Pi_e = \Pi - \Pi_c$ in Eq. (4), is expressed by

$$\begin{aligned}\Pi_e = \frac{1}{2}\int_0^\infty \int_0^n \Bigg[& \left(S_{11} - \frac{S_{12}^2}{S_{22}}\right)\left(\sigma_r^e\right)^2 + \left(S_{33} - \frac{S_{23}^2}{S_{22}}\right)\left(\sigma_z^e\right)^2 \\ & + \left(S_{66} - \frac{S_{26}^2}{S_{22}}\right)\left(\tau_{r\theta}^e\right)^2 + S_{44}\left(\tau_{zr}^e\right)^2 + S_{55}\left(\tau_{z\theta}^e\right)^2 \\ & + 2\left(S_{13} - \frac{S_{12}S_{23}}{S_{22}}\right)\left(\sigma_r^e\right)\left(\sigma_z^e\right) + 2\left(S_{16} - \frac{S_{12}S_{26}}{S_{22}}\right)\left(\sigma_r^e\right)\left(\tau_{r\theta}^e\right) \\ & + 2\left(S_{36} - \frac{S_{23}S_{26}}{S_{22}}\right)\left(\sigma_z^e\right)\left(\tau_{r\theta}^e\right) + 2S_{45}\left(\tau_{zr}^e\right)\left(\tau_{z\theta}^e\right) + 2\left(\sigma_r^e\right)\left(\varepsilon_r^c\right) \\ & + 2\left(-\frac{S_{12}}{S_{22}}\sigma_r^e - \frac{S_{23}}{S_{22}}\sigma_z^e - \frac{S_{26}}{S_{22}}\tau_{r\theta}^e\right)\left(\varepsilon_\theta^c\right) + 2\left(\tau_{r\theta}^e\right)\left(\varepsilon_{r\theta}^c\right)\Bigg] h^2 \, \mathrm{d}\xi \, \mathrm{d}\eta \end{aligned} \tag{21}$$

Substituting the expressions for boundary-layer stress components into Eq. (21) and integrating with respect to η in the interval $0 \leq \eta \leq n$, the complementary energy of the system Π_e is obtained only in terms of functions Φ and Ψ:

$$\Pi_e = h^2 \int_0^\infty \Gamma(\Phi, \Phi', \Phi'', \Psi, \Psi') \, \mathrm{d}\xi \tag{22}$$

where

$$\begin{aligned}\Gamma(\Phi, \Phi', \Phi'', \Psi, \Psi') = {} & f_1\Phi^2 + f_2(\Phi'')^2 + f_3\Psi^2 + f_4(\Phi')^2 \\ & + f_5(\Psi')^2 + f_6\Phi\Phi'' + f_7\Phi\Psi + f_8\Phi''\Psi + f_9\Phi'\Psi' \\ & + f_{10}\varepsilon_\theta^c\Phi + f_{11}\varepsilon_\theta^c\Psi + f_{12}\varepsilon_\theta^c\Phi'' \end{aligned} \tag{23}$$

The parameters f_i in Eq. (23) are defined in the Appendix. The complementary energy Π_e and the function Γ are also called the functionals of the system because they are functions of other functions Φ and Ψ. Now the governing equations of the system can be yielded by invoking the stationarity condition of Π_e, i.e., $\delta\Pi_e = 0$, with respect to the two functions Φ and Ψ (Ref. 38). In addition, the boundary conditions corresponding to the prescribed displacements on the contact surfaces (namely, the natural boundary conditions defined subsequently) can be generated and taken into account using the variational principle of complementary energy. Imposing variations onto Eq. (22) and applying the traction-free boundary conditions (namely, the essential boundary conditions defined subsequently) in Eqs. (19), one can obtain two Euler–Lagrange equations,

$$\frac{\partial\Gamma}{\partial\Phi} - \frac{\mathrm{d}}{\mathrm{d}\xi}\left(\frac{\partial\Gamma}{\partial\Phi'}\right) + \frac{\mathrm{d}^2}{\mathrm{d}\xi^2}\left(\frac{\partial\Gamma}{\partial\Phi''}\right) = 0 \tag{24}$$

$$\frac{\partial\Gamma}{\partial\Psi} - \frac{\mathrm{d}}{\mathrm{d}\xi}\left(\frac{\partial\Gamma}{\partial\Psi'}\right) = 0 \tag{25}$$

The natural boundary condition is obtained as

$$\left[\frac{\partial\Gamma}{\partial\Phi'} - \frac{\mathrm{d}}{\mathrm{d}\xi}\left(\frac{\partial\Gamma}{\partial\Phi''}\right)\right]\Bigg|_{\xi=0} = 0 \tag{26}$$

Substituting Eq. (23) into Eqs. (24–26), the following equations in which functions Φ and Ψ yield stationarity of the complementary energy are derived:

$$\begin{aligned} & 2f_1\Phi + 2(f_6 - f_4)\phi'' + (f_8 - f_9)\Psi'' + f_7\Psi \\ & \quad + 2f_2\Phi^{IV} + f_{10}\varepsilon_\theta^c + f_{12}\left(\varepsilon_\theta^c\right)'' = 0 \end{aligned} \tag{27}$$

$$2f_3\Psi + f_7\Phi + (f_8 - f_9)\Phi'' - 2f_5\Psi'' + f_{11}\varepsilon_\theta^c = 0 \tag{28}$$

$$2f_2\Phi'''(0) + (f_8 - f_9)\Psi'(0) = -f_{12}\left(\varepsilon_\theta^c\right)'\Big|_{\xi=0} \tag{29}$$

Combining Eqs. (27) and (28) leads to

$$\Phi^{VI} + g_1\Phi^{IV} + g_2\Phi'' + g_3\Phi = -g_4\varepsilon_\theta^c - g_5\left(\varepsilon_\theta^c\right)'' - g_6\left(\varepsilon_\theta^c\right)^{IV} \tag{30}$$

$$\Psi = h_1\Phi^{IV} + h_2\Phi'' + h_3\Phi + h_4\varepsilon_\theta^c + h_5\left(\varepsilon_\theta^c\right)'' \tag{31}$$

where g_i and h_i are θ-dependent parameters to be expressed in the Appendix. Thus, the general solutions for Φ and Ψ are determined through the parameters g_i by the CLPT stress components of individual plies along the pin-loaded hole edges. The terms related to the CLPT circumferential strain ε_θ^c around the holes constitute particular solutions, which thus attain a value of zero far away from the pin-loaded holes. From the sixth-order linear differential equation (30), the general and particular solutions of Φ are obtained by using the standard procedure of linear differential equations with the functions represented in terms of exponentials. The function Ψ is simultaneously obtained from Eq. (31). The general solution for Eq. (30) is obtained, using the following characteristic equation:

$$\lambda^6 + g_1\lambda^4 + g_2\lambda^2 + g_3 = 0 \tag{32}$$

For general cases, the boundary-layer stresses can be represented by two functions. But in some special cases, some boundary-layer

stress components are identically equal to zero. For example, if the CLPT component $\tau_{r_\theta}^{c(i)}$ vanish in each ply, the stress components $\tau_{r_\theta}^{e(i)}$ and $\tau_{z_\theta}^{e(i)}$ are always equal to zero due to the assumption in Eq. (18). These situations may be encountered in cross-ply laminates. Thus, the boundary-layer stresses are related to one function Φ and Eqs. (27) and (29) are degenerated into

$$\Phi^{IV} + \frac{f_6 - f_4}{f_2}\Phi'' + \frac{f_1}{f_2}\Phi = -\frac{f_{10}\varepsilon_\theta^c + f_{12}\left(\varepsilon_\theta^c\right)''}{2f_2} \tag{33}$$

$$2f_2\Phi'''(0) = -f_{12}\left(\varepsilon_\theta^c\right)'\big|_{\xi=0} \tag{34}$$

and the related characteristic equation is

$$\lambda^4 + \frac{f_6 - f_4}{f_2}\lambda^2 + \frac{f_1}{f_2} = 0 \tag{35}$$

Solutions to the Problem

The solution forms for functions Φ and Ψ are determined by the roots of characteristic equations, which vary with different material properties and laminate constructions. Also, the roots are not constants but dependent on the values of θ; therefore, even for a given laminate, the solutions have different forms at different θ. The following solution cases will be encountered in the numerical examples of next section.

A. Case 1

The solution of characteristic equation (32) has two real roots and four complex roots:

$$\lambda_{1,2} = \pm\alpha, \qquad \lambda_{3,4,5,6} = \pm(\beta \pm \gamma i) \tag{36}$$

where α, β, and γ are positive and real. The general solution for Φ involves terms with $e^{\pm\alpha\xi}$, $e^{\pm\beta\xi}\sin\gamma\xi$, and $e^{\pm\beta\xi}\cos\gamma\xi$. To ensure that edge effects disappear and the results of the CLPT are recovered far from the boundaries [functionally expressed in Eqs. (19c) and (19d)], the terms with positive exponential must be neglected. Thus, the complete solution of Φ is

$$\Phi(\xi) = C_1 e^{-\alpha\xi} + C_2 e^{-\beta\xi}\sin\gamma\xi + C_3 e^{-\beta\xi}\cos\gamma\xi + \Phi_1(\xi) \tag{37}$$

where C_1, C_2, and C_3 are parameters involved in the general solution of Φ, and Φ_1 is the particular solution. Simultaneously, substituting the expression of Φ into Eq. (31), the complete solution of Ψ is obtained as

$$\Psi(\xi) = I_1 C_1 e^{-\alpha\xi} + (I_3 C_2 - I_2 C_3) e^{-\beta\xi}\sin\gamma\xi + (I_2 C_2 + I_3 C_3) e^{-\beta\xi}\cos\gamma\xi + \Psi_1(\xi) \tag{38}$$

where

$$I_1 = \alpha^4 h_1 + \alpha^2 h_2 + h_3 \tag{39a}$$

$$I_2 = -2\beta\gamma\left[2(\beta^2 - \gamma^2)h_1 + h_2\right] \tag{39b}$$

$$I_3 = (\beta^4 + \gamma^4 - 6\beta^2\gamma^2)h_1 + (\beta^2 - \gamma^2)h_2 + h_3 \tag{39c}$$

The particular solution Ψ_1 is determined to be

$$\Psi_1(\xi) = h_1\Phi_1^{IV}(\xi) + h_2\Phi_1''(\xi) + h_3\Phi_1(\xi) + h_4\varepsilon_\theta^c + h_5\left(\varepsilon_\theta^c\right)'' \tag{40}$$

Then the three parameters C_1, C_2, and C_3 can be determined by the boundary conditions at $\xi = 0$. There are three essential boundary conditions in Eq. (19b) on the no-contact surface and two essential boundary conditions in Eq. (19a) and one natural condition in Eq. (29) regarding the prescribed radial displacement on the contact surface. Imposing both the no-contact and contact surfaces with shear traction-free conditions, one gets the following two equations:

$$-\alpha C_1 + \gamma C_2 - \beta C_3 = -\Phi_1'(0) \tag{41a}$$

$$I_1 C_1 + I_2 C_2 + I_3 C_3 = -1 - \Psi_1(0) \tag{41b}$$

The no-contact surface with the radial traction-free condition yields the equation

$$C_1 + C_3 = -1 - \Phi_1(0) \tag{41c}$$

and the contact surface with the natural boundary condition yields the following equation:

$$\begin{aligned}&\left[I_1\alpha(f_8 - f_9) + 2\alpha^3 f_2\right]C_1 \\ &\quad - \left[(I_3\gamma - I_2\beta)(f_8 - f_9) + 2f_2(3\beta^2\gamma - \gamma^3)\right]C_2 \\ &\quad - \left[-(I_3\beta + I_2\gamma)(f_8 - f_9) + 2f_2(3\beta\gamma^2 - \beta^3)\right]C_3 \\ &\quad = f_{12}\left(\xi_\theta^c\right)'\big|_{\xi=0} + 2f_2\Phi_1'''(0) + (f_8 - f_9)\Psi_1'(0)\end{aligned} \tag{41d}$$

Equations (41a–41c) are combined to solve the parameters for the region inside the no-contact angle, and Eqs. (41a), (41b), and (41d) are combined to solve the parameters for the region inside the contact angle.

B. Case 2

The solution of Eq. (32) has six real roots,

$$\lambda_{1,2} = \pm\alpha, \qquad \lambda_{3,4} = \pm\beta, \qquad \lambda_{5,6} = \pm\gamma \tag{42}$$

For the same reasons given for case 1, positive roots are neglected, and the complete solution for Φ is

$$\Phi(\xi) = C_1 e^{-\alpha\xi} + C_2 e^{-\beta\xi} + C_3 e^{-\gamma\xi} + \Phi_1(\xi) \tag{43}$$

Through Eq. (31), the complete solution for Ψ is obtained as

$$\Psi(\xi) = I_1 C_1 e^{-\alpha\xi} + I_2 C_2 e^{-\beta\xi} + I_3 C_3 e^{-\gamma\xi} + \Psi_1(\xi) \tag{44}$$

where the particular solution Ψ_1 has the same form as that in Eq. (40) and, furthermore,

$$I_1 = \alpha^4 h_1 + \alpha^2 h_2 + h_3 \tag{45a}$$

$$I_2 = \beta^4 h_1 + \beta^2 h_2 + h_3 \tag{45b}$$

$$I_3 = \gamma^4 h_1 + \gamma^2 h_2 + h_3 \tag{45c}$$

Imposing the essential boundary conditions on the hole edge, one obtains the following two equations on both the no-contact surface and the contact surface:

$$-\alpha C_1 - \beta C_2 - \gamma C_3 = -\Phi_1'(0) \tag{46a}$$

$$I_1 C_1 + I_2 C_2 + I_3 C_3 = -1 - \Psi_1(0) \tag{46b}$$

and the following equation on the no-contact surface:

$$C_1 + C_2 + C_3 = -1 - \Phi_1(0) \tag{46c}$$

In addition, on the contact surface

$$\begin{aligned}&\left[I_1\alpha(f_8 - f_9) + 2\alpha^3 f_2\right]C_1 + \left[I_2\beta(f_8 - f_9) + 2\beta^3 f_2\right]C_2 \\ &\quad + \left[I_3\gamma(f_8 - f_9) + 2\gamma^3 f_2\right]C_3 = f_{12}\left(\varepsilon_\theta^c\right)'\big|_{\xi=0} + 2f_2\Phi_1'''(0) \\ &\quad + (f_8 - f_9)\Psi_1'(0)\end{aligned} \tag{46d}$$

Similarly, Eqs. (46a–46c) are then combined to determine the three parameters for the region inside the no-contact angle, and Eqs. (41a), (41b), and (41d) are combined to determine the three parameters for the region inside the contact angle.

C. Case 3

When the solution of characteristic equation (35) has four complex roots

$$\lambda_{1,2,3,4} = \pm(\alpha \pm \beta i) \tag{47}$$

then the complete solution for Φ is

$$\Phi(\xi) = C_1 e^{-\alpha\xi} \sin\beta\xi + C_2 e^{-\alpha\xi} \cos\beta\xi + \Phi_1(\xi) \tag{48}$$

The shear traction-free condition $\Phi'(0) = 0$ on both the contact and no-contact surfaces yields

$$\beta C_1 - \alpha C_2 = -\Phi_1'(0) \tag{49a}$$

The radial traction-free condition $\Phi(0) = -1$ on the no-contact surface yields

$$C_2 = -1 - \Phi_1(0) \tag{49b}$$

The natural boundary condition regarding $u_r^{(i)}(0) = u_{r0}^c$ on the contact surface yields

$$2f_2(3\alpha^2\beta - \beta^3)C_1 + 2f_2(3\alpha\beta^2 - \alpha^3)C_2 = -f_{12}\left(\varepsilon_\theta^c\right)'\big|_{\xi=0} - 2f_2\Phi_1'''(0) \tag{49c}$$

Thus, the set of Eqs. (49a) and (49b) yields the two parameters for the region inside the no-contact angle, and the set of Eqs. (49a) and (49c) yields the two parameters for the region inside the contact angle.

Therefore, if the CLPT stress and strain states around the pin-loaded holes are known a priori, the procedure to determine the complete solutions of Φ and Ψ poses no mathematical difficulty in the present model. It is clear that the θ dependence of boundary-layer stresses arise from the CLPT stress components through the assumptions in Eqs. (17) and (18) and the roots of characteristic equations through parameters f_i, which are governed by both compliances S_{ij} and the CLPT stress components.

Numerical Examples and Discussions

The analytical solution outlined in the foregoing is applied to study interlaminar stresses around pin-loaded holes in cross-ply graphite/epoxy laminates. A quantitative comparison with the linear finite element results obtained by Lessard et al.[23] and Shokrieh and Lessard[7] is also provided. For the purpose of comparison, the load P is applied to the laminate along one of its principal axes in the numerical examples, that is, the principal axes of the laminate are coincided with the x and y axes, as shown in Fig. 1. Consistent with the boundary conditions in the finite element models,[7,23] the rigid pins are assumed to have the same diameter as the holes, thus forming perfect fitting between them. The basic material properties of the graphite/epoxy system considered in the work of Lessard et al.[23] are adopted: $E_{11} = 150$ GPa, $E_{22} = E_{33} = 8$ GPa, $G_{12} = G_{13} = 5$ GPa, $G_{23} = 3$ GPa, $\nu_{12} = \nu_{13} = \nu_{23} = 0.3$, and $h = 0.134$ mm. The thickness of all of the considered laminates is $H = 2.144$ mm (composed of 16 plies), and the radius of the pin-loaded hole in each laminate is $R = 3.175$ mm. In the results discussed, all of the stresses are normalized with respect to the bearing stress σ_b, which is equal to $P/(2RH)$.

To obtain the CLPT stress and strain states around pin-loaded holes, Zhang and Ueng's compact analytical solutions[30] in the forms of Lekhnitskii's complex stress functions are chosen because a clear analytical solution form for both average in-plane stresses and displacements along the hole edges can be easily derived from the complex stress functions. The determination of average in-plane stress and strain states near the pin-loaded holes from the complex stress functions, however, is algebraically tedious. To overcome this difficulty, a simplified technique[39] is adopted, in which the radial distribution of average in-plane stresses are approximately represented in terms of exponentials associated with their corresponding values at the hole edges. From the simplified technique, the circumferential in-plane strain of the laminates around pin-loaded holes can be approximated as

$$\varepsilon_\theta^c = \varepsilon_{\theta 0}^c e^{-\kappa\xi} \tag{50}$$

where κ is a nondimensional constant dependent on laminate geometry and construction and contact characteristic, thereby making it rather convenient to determine the particular solutions Φ_1 and Ψ_1. The exponentials are believed to provide a better approximation because the average in-plane stresses vanish monotonically away from the holes.[39] The values of κ are 4.72×10^{-2} for the cross-ply laminates in the present numerical examples. The CLPT stress and strain states required as primitive input data in the present solutions are calculated from Zhang and Ueng's solutions,[30] where the region of contact surfaces has been set to be $-90 \le \theta \le 90$ deg, i.e., semihole contact. As a result, this contact region is used in the present numerical examples. In many existing works,[7,23] a smaller contact region, such as $-82.5 \le \theta \le 82.5$ deg, has been considered to be more reasonable for the composite pinned joints with perfect fitting. Therefore, the following numerical results are demonstrated only in the laminates within the region of $0 \le \theta \le 90$ deg because the edge effects in the vicinity of no-contact surfaces are small compared with those in the vicinity of contact surfaces. In the problem of free edge effects using a similar procedure of complementary energy principle,[19,20,28] the particular solutions in the stress functions are abandoned to simplify the formulations, which seems to have little effect on the numerical results. Accordingly, the influences of the particular solutions Φ_1 and Ψ_1 on the edge effects in the present model are examined here.

The in-plane stress components in the 0- and 90-deg layers of a $[0_4/90_4]_s$ laminate along the pin-loaded hole edge are shown in Figs. 3 and 4 to substantiate the validity of the present model. The CLPT stress results are calculated using Zhang and Ueng's

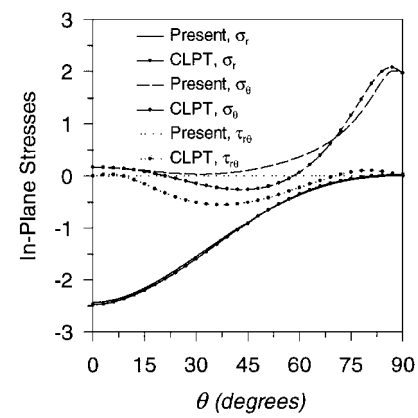

Fig. 3 In-plane stresses along the pin-loaded hole edge in the 0-deg layer of a $[0_4/90_4]_s$ laminate; CLPT stresses are based on Zhang and Ueng's solutions.[30]

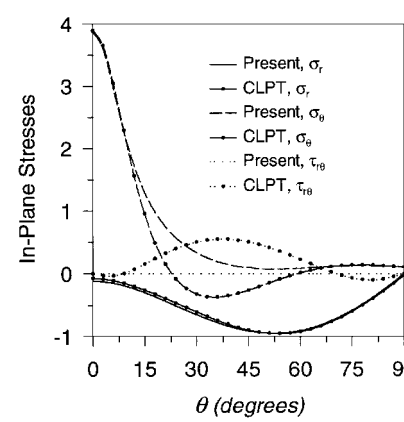

Fig. 4 In-plane stresses along the pin-loaded hole edge in the 90-deg layer of a $[0_4/90_4]_s$ laminate; CLPT stresses are based on Zhang and Ueng's solutions.[30]

analytical solutions.[30] The present stress results are calculated using the stress functions with particular solutions Φ_1 and Ψ_1 included, and the circumferential stress σ_θ is the average value across the layer thickness in each layer because it is not of uniform distribution along the thickness direction in the present model. It can be observed that the radial component σ_r from the two types of solutions is almost identical, although evident differences for the other two components σ_θ and τ_{r_θ} are present. In particular, the shear stress τ_{r_θ} from the present solutions is identically equal to zero on the contact surfaces, but it is quite large from the CLPT solutions. Hence, the traction boundary conditions on the contact surfaces are exactly satisfied in the present solutions. Thus, it can be seen that the present solutions provide an improvement over the CLPT solutions.

Figures 5–7 show the circumferential distribution of the interlaminar stresses at the 0/90 interface right at the pin-loaded hole edge in a $[0_4/90_4]_s$ laminate, wherein the results from the present solutions with or without consideration of the particular solutions Φ_1 and Ψ_1 in the stress functions are compared with the three-dimensional linear finite element results obtained by Lessard et al.[23] and Shokrieh and Lessard.[7] In the finite element analysis, the interlaminar stress values near pin-loaded hole edges are very sensitive to the element meshing. As a matter of fact, Lessard et al.[23] predicted a much higher interlaminar shear stress concentration through a fine element meshing, whereas Shokrieh and Lessard[7] predicted a lesser stress concentration through a relatively coarse element meshing. It is seen from Figs. 5 and 6 that, when the stress functions with particular solutions included are considered, not only the stress values but also the variation trend seem to tend toward the results obtained in Lessard et al.[23] Hence, the inclusion of particular solutions into the stress functions, i.e., complete solutions in the present model, is quite important. The interlaminar shear stress values predicted by the present solutions lie between those by the two finite element solutions.[7,23] Because of the existence of the potentially high interlaminar stress gradient field near the edges, different methods may predict different peak stress values at the edges.[34] For example, it is believed that higher interlaminar stresses concentrations can be predicted if the displacement continuity at ply interfaces is exactly satisfied.[40] Therefore, the present model based on the variational principle of complementary energy may predict stress values with a lower level of concentration along hole edges. The interlaminar shear stresses obtained using the present solutions, however, have a good correlation with the finite element results[7,23] except within a small region near $\theta = 90$ deg. This discrepancy results from the difference in the contact angles used in the finite element analysis (wherein the contact region was set to be $-82.5 \le \theta \le 82.5$ deg) (Ref. 23) and in Zhang and Ueng's solutions.[30] The present results and the finite element results[23] in Fig. 7 show considerable differences in the case of the interlaminar normal stress σ_z, especially near the contact center (at $\theta = 0$ deg), though the value and location of negative peak stress predicted by the two solutions are fairly close. In fact, it seems more difficult to obtain the accurate value of interlaminar normal stress arising from edge effects.[14,19,37] Even for the simple case of straight free edges in $[45/45]_s$ angle-ply laminate, the interlaminar normal stress disagrees in both magnitude and sign from various analytical models.[14] Fortunately, the magnitude of σ_z is comparatively small in this problem.

The edge effects around pin-loaded holes in a $[90_4/0_4]_s$ laminate are also analyzed by the present solutions. Only the interlaminar stress σ_z at the 90/0 interface along the pin-loaded hole edge is presented in Fig. 8 because the results indicate that the magnitudes of interlaminar shear stresses $\tau_{z\theta}$ and τ_{zr} are identical for both $[90_4/0_4]_s$ and $[0_4/90_4]_s$ laminates. To make further comparison, the finite element results for a $[90_2/0_2]_s$ laminate obtained from Sperling[21] are also included in Fig. 8, although the material properties are somewhat different and the hole size and laminate thickness are not reported. The results for the stress σ_z from the present solution and the finite element analysis[23] reach a good agreement except within the region near $\theta = 90$ deg because of different contact angles in these two solutions. However, they do not agree with those of Shokrieh

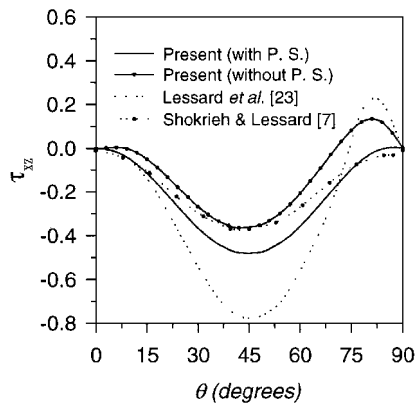

Fig. 5 Interlaminar shear stress τ_{xz} at the 0/90 interface along the pin-loaded hole edge in a $[0_4/90_4]_s$ laminate. P.S., particular solution.

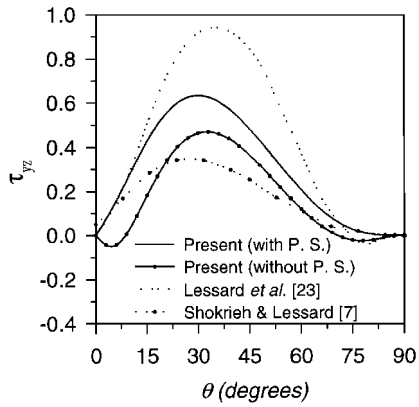

Fig. 6 Interlaminar shear stress τ_{yz} at the 0/90 interface along the pin-loaded hole edge in a $[0_4/90_4]_s$ laminate. P.S., particular solution.

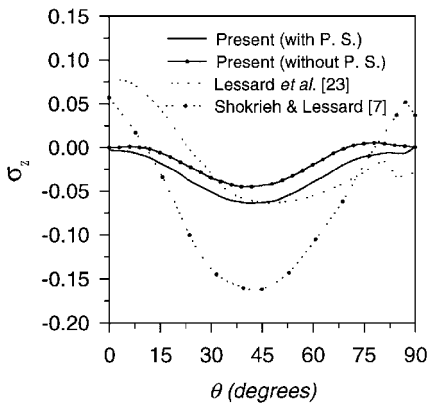

Fig. 7 Interlaminar normal stress σ_z at the 0/90 interface along the pin-loaded hole edge in a $[0_4/90_4]_s$ laminate. P.S., particular solution.

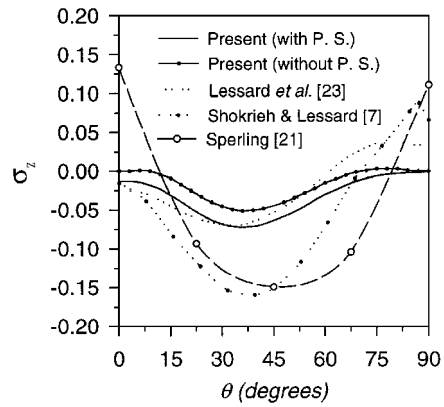

Fig. 8 Interlaminar normal stress σ_z at the 90/0 interface along the pin-loaded hole edge in a $[90_4/0_4]_s$ laminate. P.S., particular solution.

and Lessard[7] and Sperling.[21] It is especially noticeable that interlaminar tensile normal stress with a higher value near $\theta = 0$ deg is predicted by Sperling.[21] This discrepancy may be attributed to the element meshing in the finite element analysis because the magnitudes of concentrated interlaminar stresses along the hole edges strongly depend on the mesh size. Comparing the finite element results in various papers,[7,21–23] interesting evidence may be discovered that, for the cross-ply laminates, the finite element models with coarse meshing predict lower interlaminar shear stresses but higher normal stress. The radial distribution of all of the three interlaminar stresses at the 90/0 interface in the $[90_4/0_4]_s$ laminate is provided through a range of θ values with the aid of the complete solutions of the stress functions in the present model, as shown in Figs. 9–11. It is seen that the component $\tau_{z\theta}$ is dominant around the pin-loaded holes and the magnitude of the other two components τ_{zr} and σ_z are much smaller. The edge effects characteristically with high-stress

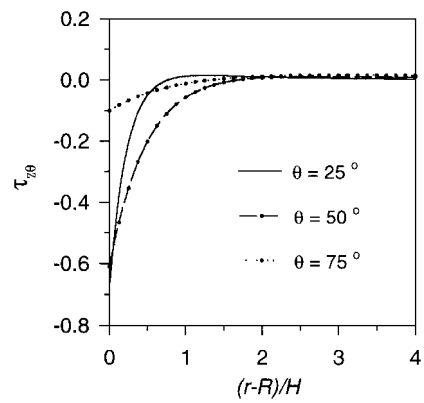

Fig. 9 Radial distribution of interlaminar shear stress $\tau_{z\theta}$ at the 90/0 interface around the pin-loaded hole in a $[90_4/0_4]_s$ laminate.

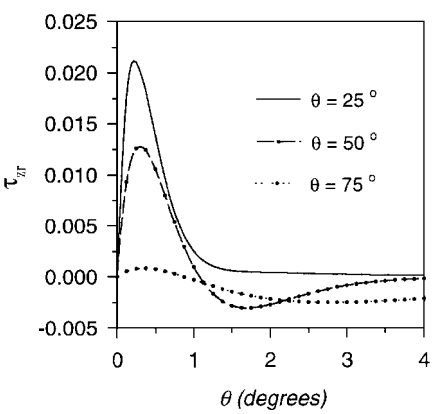

Fig. 10 Radial distribution of interlaminar shear stress τ_{zr} at the 90/0 interface around the pin-loaded hole in a $[90_4/0_4]_s$ laminate.

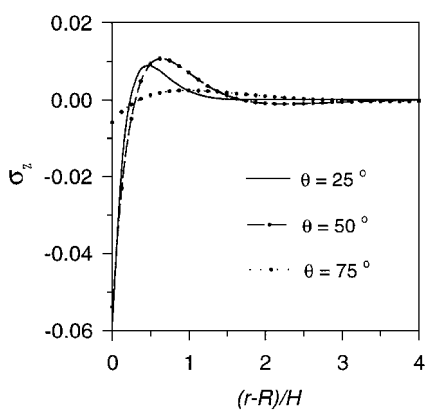

Fig. 11 Radial distribution of interlaminar normal stress σ_z at the 90/0 interface around the pin-loaded hole in a $[90_4/0_4]_s$ laminate.

gradient are localized within about two laminate thickness distance away from the hole edges, and the stresses $\tau_{z\theta}$ and σ_z vanish more quickly than the stress τ_{zr}. The sign of all three interlaminar stresses is changed, but the radial die-away distribution of the component $\tau_{z\theta}$ is close to a monotonic type. An important evidence observed is that the edge effects disappear more rapidly at locations close to the contact center.

Conclusions

An analytical technique has been developed to yield closed-form solutions for the edge effect stresses around pin-loaded holes in laminated composites. From the present solutions, the three-dimensional stress state resulting from the edge effects can conveniently be determined based on the knowledge of in-plane stresses and strains around the pin-loaded holes, which can be obtained with the CLPT. In addition, the present solutions for the region inside the no-contact angle can be extended to calculate the free edge effects around traction-free circular holes. Following the numerical results in the preceding section, the following can be concluded:

1) The edge effects have strong influence on the in-plane stresses σ_θ and $\tau_{r\theta}$ but have less influence on the in-plane radial stress σ_r around pin-loaded holes.

2) The edge effects vanish more quickly near the center of the contact surface, but the maximum interlaminar stress state exists at points not far away from the contact center.

3) The stress component $\tau_{z\theta}$ is much larger than the other two interlaminar stress components.

4) The particular solutions should be included in the stress functions to improve the precision of numerical results but can be neglected to further reduce the involved mathematical work when making qualitative comparison for design scheme.

5) The present technique can efficiently calculate the three-dimensional edge effect stresses in thick laminates because the solutions are given in closed forms.

Appendix: Parameters Used in Complementary Energy Function

The following expressions define the parameters f_i, g_i, and h_i involved in the formulations of the text: The expressions for f_i are

$$f_1 = \frac{1}{2}\sum_{i=1}^{n}\left(S_{11}^{(i)} - \frac{S_{12}^{(i)^2}}{S_{22}^{(i)}}\right)\left(\sigma_{r0}^{c(i)} - \sigma_{r0}^{c}\right)^2 \tag{A1}$$

$$f_2 = \frac{1}{2}\sum_{i=1}^{n}\left(S_{33}^{(i)} - \frac{S_{23}^{(i)^2}}{S_{22}^{(i)}}\right)\left\{\frac{1}{20}[i^5-(i-1)^5] + \frac{1}{3}A^{(i)^2}[i^3-(i-1)^3] + B^{(i)^2} + \frac{1}{4}A^{(i)}[i^4-(i-1)^4] + \frac{1}{3}B^{(i)}[i^3-(i-1)^3] + A^{(i)}B^{(i)}[i^2-(i-1)^2]\right\}\left(\sigma_{r0}^{c(i)} - \sigma_{r0}\right)^2 \tag{A2}$$

$$f_3 = \frac{1}{2}\sum_{i=1}^{n}\left(S_{66}^{(i)} - \frac{S_{26}^{(i)^2}}{S_{22}^{(i)}}\right)\left(\tau_{r\theta 0}^{c(i)}\right)^2 \tag{A3}$$

$$f_4 = \frac{1}{2}\sum_{i=1}^{n} S_{44}^{(i)}\left\{\frac{1}{3}[i^3-(i-1)^3] + A^{(i)}[i^2-(i-1)^2] + A^{(i)^2}\right\} \times \left(\sigma_{r0}^{c(i)} - \sigma_{r0}^{c}\right)^2 \tag{A4}$$

$$f_5 = \frac{1}{2}\sum_{i=1}^{n} S_{55}^{(i)}\left\{\frac{1}{3}[i^3-(i-1)^3] + C^{(i)}[i^2-(i-1)^2] + C^{(i)^2}\right\} \times \left(\tau_{r\theta 0}^{c(i)}\right)^2 \tag{A5}$$

$$f_6 = \sum_{i=1}^{n}\left(S_{13}^{(i)} - \frac{S_{12}^{(i)}S_{23}^{(i)}}{S_{22}^{(i)}}\right)\left\{\frac{1}{6}[i^3-(i-1)^3] + \frac{1}{2}A^{(i)}[i^2-(i-1)^2] + B^{(i)}\right\}\left(\sigma_{r0}^{c(i)} - \sigma_{r0}^{c}\right)^2 \tag{A6}$$

$$f_7 = \sum_{i=1}^{n} \left(S_{16}^{(i)} - \frac{S_{12}^{(i)} S_{26}^{(i)}}{S_{22}^{(i)}} \right) \left(\sigma_{r0}^{c(i)} - \sigma_{r0}^{c} \right) \left(\tau_{r\theta 0}^{c(i)} \right) \tag{A7}$$

$$f_8 = \sum_{i=1}^{n} \left(S_{36}^{(i)} - \frac{S_{23}^{(i)} S_{26}^{(i)}}{S_{22}^{(i)}} \right) \left\{ \frac{1}{6}[i^3 - (i-1)^3] + \frac{1}{2} A^{(i)}[i^2 - (i-1)^2] + B^{(i)} \right\} \left(\sigma_{r0}^{c(i)} - \sigma_{r0}^{c} \right) \left(\tau_{r\theta 0}^{c(i)} \right) \tag{A8}$$

$$f_9 = \sum_{i=1}^{n} S_{45}^{(i)} \left\{ \frac{1}{3}[i^3 - (i-1)^3] + \frac{1}{2}(A^{(i)} + C^{(i)})[i^2 - (i-1)^2] + A^{(i)} C^{(i)} \right\} \left(\sigma_{r0}^{c(i)} - \sigma_{r0}^{c} \right) \left(\tau_{r\theta 0}^{c(i)} \right) \tag{A9}$$

$$f_{10} = -\sum_{i=1}^{n} \frac{S_{12}^{(i)}}{S_{22}^{(i)}} \left(\sigma_{r0}^{c(i)} - \sigma_{r0}^{c} \right) \tag{A10}$$

$$f_{11} = -\sum_{i=1}^{n} \frac{S_{26}^{(i)}}{S_{22}^{(i)}} \tau_{r\theta 0}^{c(i)} \tag{A11}$$

$$f_{12} = -\sum_{i=1}^{n} \frac{S_{23}^{(i)}}{S_{22}^{(i)}} \left\{ \frac{1}{6}[i^3 - (i-1)^3] + \frac{1}{2} A^{(i)}[i^2 - (i-1)^2] + B^{(i)} \right\} \times \left(\sigma_{r0}^{c(i)} - \sigma_{r0}^{c} \right) \tag{A12}$$

The parameters for g_i are

$$g_1 = \frac{(f_8 - f_9)^2 + 4 f_5 (f_6 - f_4) - 4 f_2 f_3}{\Delta} \tag{A13}$$

$$g_2 = \frac{4 f_1 f_5 + 2 f_7 (f_8 - f_9) - 4 f_3 (f_6 - f_4)}{\Delta} \tag{A14}$$

$$g_3 = \frac{f_7^2 - 4 f_1 f_3}{\Delta} \tag{A15}$$

$$g_4 = \frac{f_7 f_{11} - 2 f_3 f_{10}}{\Delta} \tag{A16}$$

$$g_5 = \frac{2 f_5 f_{10} + f_{11} (f_8 - f_9) - 2 f_3 f_{12}}{\Delta} \tag{A17}$$

$$g_6 = \frac{2 f_5 f_{12}}{\Delta} \tag{A18}$$

where

$$\Delta = 4 f_2 f_5 \tag{A19}$$

The parameters for h_i are

$$h_1 = \frac{4 f_2 f_5}{\Delta^*} \tag{A20}$$

$$h_2 = \frac{(f_8 - f_9)^2 + 4 f_5 (f_6 - f_4)}{\Delta^*} \tag{A21}$$

$$h_3 = \frac{4 f_1 f_5 + f_7 (f_8 - f_9)}{\Delta^*} \tag{A22}$$

$$h_4 = \frac{2 f_5 f_{10} + f_{11} (f_8 - f_9)}{\Delta^*} \tag{A23}$$

$$h_5 = \frac{2 f_5 f_{12}}{\Delta^*} \tag{A24}$$

where

$$\Delta^* = -2[f_5 f_7 + f_3 (f_8 - f_9)] \tag{A25}$$

Acknowledgment

Financial support from the Natural Sciences and Engineering Research Council of Canada is gratefully appreciated.

References

[1]Quinn, W. J., and Matthews, F. L., "The Effect of Stacking Sequence on the Pin-Bearing Strength in Glass Fibre Reinforced Plastic," *Journal of Composite Materials*, Vol. 11, April 1977, pp. 139–145.

[2]Chang, F. K., Scott, R. A., and Springer, G. S., "Strength of Mechanically Fastened Composite Joints," *Journal of Composite Materials*, Vol. 16, Nov. 1982, pp. 470–494.

[3]Chang, F. K., and Chang, K. Y., "Post-Failure Analysis of Bolted Joints in Tension or Shear-Out Mode Failure," *Journal of Composite Materials*, Vol. 21, Sept. 1987, pp. 809–833.

[4]Hung, C. L., and Chang, F. K., "Bearing Failure of Bolted Composite Joints," *Journal of Composite Materials*, Vol. 30, No. 12, 1996, pp. 1359–1400.

[5]Matthews, F. L., Wong, C. M., and Chryssafitis, S., "Stress Distribution Around a Single Bolt in Fiber-Reinforced Plastic," *Composites*, Vol. 13, July 1982, pp. 316–322.

[6]de Jong, T., "Stresses Around Pin-Loaded Holes in Composite Materials," *Proceedings of the IUTAM Symposium on Mechanics of Composite Materials*, Blacksburg, VA, 1982, pp. 339–353.

[7]Shokrieh, M. M., and Lessard, L. B., "Effects of Material Nonlinearity on the Three-Dimensional Stress State of Pin-Loaded Composite Laminates," *Journal of Composite Materials*, Vol. 30, No. 7, 1996, pp. 839–861.

[8]Rybicki, E. F., and Schmueser, D. W., "Effect of Stacking Sequence and Lay-up Angle on Free Edge Stresses Around a Hole in a Laminated Plate Under Tension," *Journal of Composite Materials*, Vol. 12, July 1978, pp. 300–313.

[9]Lucking, W. M., Hoa, S. V., and Sankar, T. S., "The Effect of Geometry on Interlaminar Stresses of $[0/90]_s$ Composite Laminates with Circular Holes," *Journal of Composite Materials*, Vol. 18, March 1984, pp. 188–198.

[10]Ericson, K., Persson, M., Carlsson, L., and Gustavsson, A., "On the Prediction of the Initiation of Delamination in a $[0/90]_s$ Laminate with a Circular Hole," *Journal of Composite Materials*, Vol. 18, Sept. 1984, pp. 495–506.

[11]Nishioka, T., and Atluri, S. N., "Stress Analysis of Holes in Angle-Ply Laminates: An Efficient Assumed Stress 'Special-Hole-Element' Approach and a Simple Estimation Method," *Computers and Structures*, Vol. 15, No. 2, 1982, pp. 135–147.

[12]Hoa, S. V., and Feng, W., "Global/Local Approach Using Hybrid Elements for Composites," *Proceedings of 5th International Conference on Computer Aided Design in Composite Material Technology*, Udine, Italy, 1996, pp. 319–328.

[13]Spilker, R. L., and Chou, S. C., "Edge Effects in Symmetric Composite Laminates: Importance of Satisfying the Traction-Free-Edge Condition," *Journal of Composite Materials*, Vol. 14, Jan. 1980, pp. 2–20.

[14]Whitcomb, J. D., Raju, I. S., and Goree, J. G., "Reliability of the Finite Element Method for Calculating Free Edge Stresses in Composite Laminates," *Computers and Structures*, Vol. 15, No. 1, 1982, pp. 23–37.

[15]Reiss, E. L., "Extension of an Infinite Plate with a Circular Hole," *Journal of the Society for Industrial and Applied Mathematics*, Vol. 11, No. 4, 1963, pp. 840–854.

[16]Tang, S., "Interlaminar Stresses Around Circular Cutouts in Composite Plates Under Tension," *AIAA Journal*, Vol. 15, No. 11, 1977, pp. 1631–1637.

[17]Tang, S., "A Variational Approach to Edge Stresses of Circular Cutout in Composites," *Proceedings of the AIAA/ASME/ASCE/AHS 20th Structures, Structural Dynamics, and Materials Conference*, AIAA, New York, 1979, pp. 326–332.

[18]Bar-Yoseph, P., and Avrashi, J., "Interlaminar Stress Analysis for Laminated Plates Containing a Curvilinear Hole," *Computers and Structures*, Vol. 21, No. 5, 1985, pp. 917–932.

[19]Ko, C. C., and Lin, C. C., "Method for Calculating the Interlaminar Stresses in Symmetric Laminates Containing a Circular Hole," *AIAA Journal*, Vol. 30, No. 1, 1992, pp. 197–204.

[20]Zhang, C., Lessard, L. B., and Nemes, J. A., "A Closed-Form Solution for Stresses at Curved-Free-Edges in Composite Laminates—Variational Approach," *Composites Science and Technology*, Vol. 57, No. 9–10, 1997, pp. 1341–1354.

[21]Sperling, U. O., "Three-Dimensional Stress Distribution Around Pin Loaded Holes in Composite Laminates," *Proceedings of the AIAA/ASME/ASCE/AHS 26th Structures, Structural Dynamics, and Materials Conference*, AIAA, Washington, DC, 1985, pp. 743–750.

[22]Marshall, I. H., Arnold, W. S., Wood, J., and Mousley, R. F., "Observations on Bolted Connections in Composite Structures," *Composite Structures*, 1989, Vol. 13, No. 2, pp. 133–151.

[23]Lessard, L. B., Shokrieh, M. M., and Schmidt, A. S., "Three-Dimensional Stress Analysis of Composite Plates With or Without Stress Concentrations," *Proceedings of 9th International Conference on Composite Materials*, Madrid, Spain, 1993, pp. 243–250.

[24]Matthews, F. L., "Bolted Joint," *Think Composites*, edited by S. W. Tsai, 1988, Chap. 18.

[25]Hyer, M. W., and Klang, E. C., "Contact Stresses in Pin-Loaded Orthotropic Plates," *International Journal of Solids and Structures*, Vol. 21, No. 9, 1985, pp. 957–975.

[26]Lekhnitskii, G. S., *Anisotropic Plates*, Gordon and Breach, New York, 1968.

[27]Timoshenko, S., and Goodier, J. N., *Theory of Elasticity*, McGraw–Hill, New York, 1970.

[28]Kim, T., and Atluri, S. N., "Interlaminar Stresses in Composite Laminates Under Out-of-Plane Shear/Bending," *AIAA Journal*, Vol. 32, No. 8, 1994, pp. 1700–1708.

[29]Tang, S., and Levy, A., "A Boundary Layer Theory—Part II: Extension of Laminated Finite Strip," *Journal of Composite Materials*, Vol. 9, Jan. 1975, pp. 42–52.

[30]Zhang, K. D., and Ueng, C. E. S., "Stresses Around a Pin-Loaded Hole in Orthotropic Plates," *Journal of Composite Materials*, Vol. 18, Sept. 1984, pp. 432–446.

[31]de Jong, T., "Stresses Around Pin-Loaded Holes in Elastically Orthotropic or Isotropic Plates," *Journal of Composite Materials*, Vol. 11, July 1977, pp. 313–331.

[32]Raju, I. S., and Crews, J. H., Jr., "Three Dimensional Analysis of $[0/90]_s$ and $[90/0]_s$ Laminates with a Central Hole," NASA TM-83300, April 1982.

[33]Kassapoglou, C., and Lagace, P. A., "An Efficient Method for the Calculation of Interlaminar Stresses in Composite Materials," *Journal of Applied Mechanics*, Vol. 53, Dec. 1986, pp. 744–750.

[34]Kassapoglou, C., and Lagace, P. A., "Closed Form Solutions for the Interlaminar Stress Field in Angle-Ply and Cross-Ply Laminates," *Journal of Composite Materials*, Vol. 21, April 1987, pp. 292–308.

[35]Zhang, K. D., and Ueng, C. E. S., "A Simplified Approach for Interlaminar Stresses Around a Hole in $[0/90]_s$ Laminates," *Journal of Composite Materials*, Vol. 22, Feb. 1988, pp. 192–202.

[36]Lin, C. C., Hsu, C. Y., and Ko, C. C., "Interlaminar Stresses in General Laminates with Straight Free Edges," *AIAA Journal*, Vol. 33, No. 8, 1995, pp. 1471–1476.

[37]Bar-Yoseph, P., "On the Accuracy of Interlaminar Stress Calculation in Laminated Plates," *Computer Methods in Applied Mechanics and Engineering*, Vol. 36, No. 3, 1983, pp. 309–329.

[38]Reddy, J. N., *Applied Functional Analysis and Variational Methods in Engineering*, McGraw–Hill, New York, 1991.

[39]Zhang, C., Hoa, S. V., and Ganesan, R., "Approximate Solutions for Stresses Around Pin-Loaded Holes in Symmetric Composite Laminates," *Journal of Reinforced Plastics and Composites*, Vol. 17, No. 9, 1998, pp. 800–818.

[40]Hsu, P. W., and Herakovich, C. T., "A Perturbation Solution for Interlaminar Stresses in Bidirectional Laminates," *Composite Materials: Testing and Design*, ASTM STP 617, American Society for Testing and Materials, Valley Forge, PA, 1977, pp. 296–316.

A. M. Waas
Associate Editor